RESEARCH ARTICLE
Eurasian J Bio Chem Sci, 7(2):111-124, 2024
https://doi.org/10.46239/ejbcs.1517538

EJBCS

Eurasian Journal of Biological and Chemical Sciences

Journal homepage: www.dergipark.org.tr/ejbcs

Pyrazoline compounds containing different groups: Design, synthesis and comprehensive molecular docking studies

Halise Yalazan[1], Damla Koç[2], Seda Fandaklı[3], Burak Tüzün[4], Halit Kantekin[1,*]

[1]*Karadeniz Technical University, Faculty of Sciences, Department of Chemistry, Trabzon, Turkey*
[2]*Erciyes University, Faculty of Sciences, Department of Chemistry, Kayseri, Turkey*
[3]*Artvin Çoruh University, Vocational School of Health Services, Medical Laboratory Techniques Program, Artvin, Turkey*
[4]*Sivas Cumhuriyet University, Technical Sciences Vocational School of Sivas, Plant and Animal Production Department, Sivas, Turkey*

*Corresponding author : halit@ktu.edu.tr
Orcid No: https://orcid.org/0000-0003-2625-2815

Received : 17/07/2024
Accepted : 30/10/2024

To Cite / Atıf için: Yalazan H, Koç D, Fandaklı S, Tüzün B . Kantekin H. 2024. Pyrazoline compounds containing different groups: Design, synthesis and comprehensive molecular docking studies. Eurasian J Bio Chem Sci, 7(2):111-124 https://doi.org/10.46239/ejbcs.1517538

Abstract: In the presented study, a series of methoxylated pyrazoline compounds containing amine (Py_1-NH_2 and Py_2-NH_2), tosyl (Py_1-Ts and Py_2-Ts), and nitrile (Py_1-CN and Py_2-CN) group were synthesized The structures of these compounds were clarified (by MS, FT-IR, and NMR analysis) through the use of mass spectral (spectrometer), FT-IR (spectrophotometer), and NMR (spectrometer) data. In order to examine the chemical properties of methoxylated pyrazoline derivatives theoretically, calculations were performed on the B3LYP, HF, and M06-2x methods using the 6-31++g(d,p) basis set. In addition, molecular docking calculations were performed to examine the interactions of methoxylated pyrazoline derivatives against cancer proteins. Afterwards, ADME/T was performed to examine the effects of methoxylated pyrazoline derivatives as drugs on human metabolism. According to the Gaussian calculations, the Py_1-NH_2 molecule is typically more active than other molecules. However, after the molecular docking calculations, the compounds' effects on cancer proteins were examined, and it was discovered that the Py_1-NH_2 molecule had more activity overall than the others. Following a comprehensive examination of the compounds' interactions with cancer proteins, the ADME properties of the molecules were examined. According to this analysis, it would not be detrimental to use the chemicals as drugs for human metabolism.

Keywords: ADME/T, cancer, molecular docking, phthalonitrile, pyrazoline.

1. Introduction

Pyrazoline derivatives, members of the heterocyclic chemical class, are intriguing substances with a wide range of biological profiles, potential applications as drugs, and synthetic adaptability (Dipankar et. al. 2011). Many experts in the realm of medicinal chemistry have researched the pyrazoline template extensively in relation to various diseases. Numerous biological actions, including antifungal, anticancer, anti-inflammatory, antituberculosis, antidepressant, antibacterial, cholinesterase, carbonic anhydrase, and antimalarial properties, have been identified for these compounds (Altintop et. al. 2013; Çelik et. al. 2020; Kaplancıklı et. al. 2010; Kharbanda et. al. 2014; Monga et. al. 2014; Joshi et. al. 2016; Özdemir et. al. 2010; Wang et. al. 2013). In structure-activity studies on pyrazoline-based compounds, the diversity of design substitutions to the pyrazoline ring appears to have a stupendous impact on the biological profile. It has been observed by diverse researchers that the steric and electronic properties of the substituents attached to 3,5-diaryl-4,5-dihydro-1*H*-pyrazole derivatives, which represent the 2-pyrazoline class, have changed (Nehra et. al. 2020). The structurally common feature of various drugs used in the clinical treatment of many diseases is the pyrazoline ring system (Fig.1) (Bhutani et. al. 2015; Kumar et. al. 2009). Pyrazoline derivatives are used in the literature as anticancer agents in the treatment of various types of cancer (Amr et. al. 2018; Ahmed et. al. 2019; Chen et. al. 2018; Kim et. al. 2017; Li et. al. 2018; Moreno et. al. 2018; Stefanes et. al. 2019; Xu et. al. 2017).

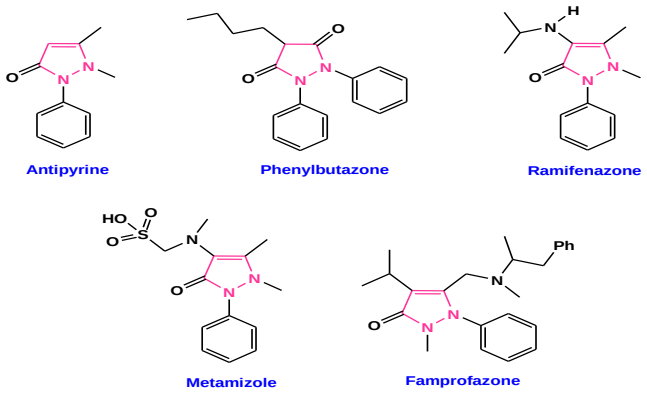

Fig. 1. Diverse pyrazoline-based clinically used drugs.

Cancer is a broad type of disease characterized by the uncontrolled, rapid, and pathological proliferation of abnormally transformed cells, and despite various alternative treatment methods developed for the treatment of this disease, cancer is still the second leading fatal disease after cardiovascular diseases all over the world. Lack of resistance and selectivity to chemotherapeutic agents are very important factors in the fight against cancer. Anticancer drugs used in the treatment of this disease destroy not only cancer cells but also normal cells, and this causes serious side effects. In order to prevent this situation, the synthesis of new antineoplastic agents that selectively destroy tumor cells or at least prevent their proliferation is constantly being developed by researchers (Nepali. et al. 2014; Nussbaumer et. al. 2011; Mathur et. al. 2015; Rebucci and Michiels 2013).

Theoretical calculations provide significant information on many aspects of molecules in addition to measuring their activity. Theoretical computations have become faster and more accurate with the advancement of technology. It is used to identify the active molecules, the portions of the molecules with the highest electron densities, and the active regions of the molecules using computations (Chalkha et. al. 2023; Majumdar et. al. 2022). The study used Gaussian calculations, B3LYP, HF, and M06-2x (Becke 1992; Hohenstein et. al. 2008; Vautherin and Brink 1972) methods using the 6-31++g(d,p) basis set to examine the chemical characteristics of the compounds. To contrast a molecule's action with biological materials, molecular docking calculations were conducted with breast cancer protein (PDB ID: 1JNX) (Williams et. al. 2001), liver cancer protein (PDB ID: 3WZE) (Okamoto et. al. 2015), prostate-specific membrane antigen (PDB ID: 6XXP) (Rosenfeld et. al. 2020), and colon cancer protein (PDB ID: 4UYA) (Marusiak et. al. 2016). Finally, the compounds' ADME/T calculations were performed, and their pharmacological characteristics were investigated.

In this study, syntheses, structural characterization, and in silico studies of methoxylated pyrazoline compounds containing amine (**Py_1-NH_2** and **Py_2-NH_2**), tosyl (**Py_1-Ts** and **Py_2-Ts**), and nitrile (**Py_1-CN** and **Py_2-CN**) groups were searched. The activities of these compounds against cancer proteins and their ADME properties were investigated. It was determined that the **Py_1-NH_2** compound showed higher activity than the other synthesized compounds.

2. Materials and Method

Every chemical that was utilized was of reagent-grade quality. Purchased from Sigma-Aldrich, Merck, and Fluka, phenylhydrazine, NaOH, p-tosyl chloride, potassium carbonate, and 4-nitrophthalonitrile were used exactly as directed. Purchased from Merck and Sigma Aldrich, the utilized solvents were used exactly as supplied.
All reactions were carried out in an oxygen-free, dry nitrogen environment using a Schlenk apparatus. The Perkin Elmer 1600 FT-IR Spectrophotometer was used to record infrared spectra. Chemical shifts were reported (δ) in the ^{1}H and ^{13}C NMR spectra recorded on a Bruker Ascent 400 MHz NMR spectrometer $CDCI_3$, using Me_4Si (tetramethylsilane) as an internal standard. A MALDI-TOF spectrometer was used to measure the mass spectra. A device known as an electrothermal was used to determine the melting points.

2.1. Synthesis

2.1.1. Methoxylated pyrazoline derivatives bearing amine group (Py_1-NH_2 and Py_2-NH_2)

Phenylhydrazine (0.54g, 5.0 mmol) was added to the solution of the appropriate chalcone-derived amine compounds (1.27g, 5.0 mmol) (**Chlcn-1**) or (1.42g, 5.0 mmol) (**Chlcn-2**) in absolute ethanol (15 mL) containing 1 g of NaOH. After heating the reaction mixture under reflux for 6–10 hours while monitoring its progress with a TLC analysis, it was allowed to cool to room temperature. The crystalline substance that had separated was filtered, then dried and cleaned with cold methanol. Hereby, the title products (**Py_1-NH_2** and **Py_2-NH_2**) were acquired as yellow solids.

2.1.1.1. 2-(5-(2-methoxyphenyl)-1-phenyl-4,5-dihydro-1H-pyrazol-3-yl)benzenamine (Py_1-NH_2)

Yield: 81%. M.p: 137−139 °C. FT-IR (ATR), υ_{max} (cm^{-1}): 3384−3291 (NH_2), 3026 (ArC−H), 2939−2844 (C−H), 1615 (C=N), 1592 (C=C), 1492−1446 (N–N), 1385, 1324, 1294, 1157, 1103, 1029, 999, 878, 736, 689. ^{1}H NMR (400 MHz, δ, ppm, DMSO-d_6): 7.12–6.56 (m,13H, Ar–H), 5.52 (bs,1H, pyrazoline-H), 3.93 (s, 3H, −OCH_3), 3.93 (bs,1H, pyrazoline-H), 3.08 (bs,1H, pyrazoline-H). APT NMR (100 MHz, δ, ppm, DMSO-d_6): N=C 156.9 (C), Ar−C [155.7 (C), 147.2 (C), 150.5 (pyrazoline-C), 144.2 (C), 143.8 (C), 129.1 (CH), 129.5 (CH), 126.4 (CH), 121.1 (CH), 118.6 (CH), 117.0 (C), 115.6 (CH), 115.5 (CH), 113.7 (C), 112.7 (CH), 111.9 (CH)], 56.3 (pyrazoline-C), 56.1 (−OCH_3), 43.7 (pyrazoline-C). MS (MALDI–TOF) *m/z*: Calculated:343.42; Found: 343.51 [M]$^+$.

2.1.1.2. 3-(5-(2,5-dimethoxyphenyl)-1-phenyl-4,5-dihydro-1H-pyrazol-3-yl)benzenamine (Py_2-NH_2)

Yield: 78%. M.p: 174−176 °C. FT-IR (ATR), υ_{max} (cm^{-1}): 3443−3361 (NH_2), 3004 (ArC−H), 2933−2834 (C−H), 1618 (C=N), 1594 (C=C), 1495−1462 (N–N), 1396, 1333, 1260, 1130, 1044, 1000, 867, 744, 687 (C−S). ^{1}H NMR (400 MHz, δ, ppm, DMSO-d_6): 6.45−7.18 (m,12H, Ar–H), 5.54 (bs,1H, pyrazoline-H), 3.86 (bs,1H, pyrazoline-H), 3.55 (s, 3H, −OCH_3), 3.40 (s, 3H, −OCH_3), 2.92 (bs, 1H,

pyrazoline-H). APT NMR (100 MHz, δ, ppm, DMSO-d_6): N=C 153.4 (C), Ar−C [150.4 (pyrazoline-C), 149.2(C), 148.7 (C), 144.8 (C), 134.8(C), 133.2(C), 130.9 (C), 129.6 (CH), 129.5 (CH), 118.7 (CH), 115.2 (CH), 114.3 (CH), 113.1 (CH), 112.9 (CH), 112.4 (CH), 111.1 (CH)], 57.9 (pyrazoline-C), 56.5 (–OCH_3), 55.4 (-OCH_3), 42.3 (pyrazoline-C). MS (MALDI–TOF) *m/z*: Calculated: 373.45; Found: 373.76 $[M]^+$.

2.1.2. Methoxylated pyrazoline derivatives bearing tosyl group (Py₁-Ts and Py₂-Ts)

Pyrazoline-derived amine compound (0.75g, 2.17 mmol) (**Py₁-NH₂**) or (0.5g, 1.34 mmol) (**Py₂-NH₂**) was solved in pyridine (20 mL), and p-tosyl chloride (0.46g, 2.39 mmol for **Py₁-Ts**) or (0.28g, 1.47 mmol for **Py₂-Ts**) dissolved in pyridine (5 mL) was added dropwise in the reaction mixture for about 1 hours. This mixture was continued at - 5–8 °C with stirring for 17 hours. The orange-colored reaction ingredients were added to crushed ice and acidified with concentrated HCl acid. The precipitated products were filtered, crystallized in ethanol, and dried in vacuo. Hereby, the title products (**Py₁-Ts** and **Py₂-Ts**) were acquired as fawn-colored solids.

2.1.2.1. N-(2-(5-(2-methoxyphenyl)-1-phenyl-4,5-dihydro-1H-pyrazol-3-yl)phenyl)-4-methyl benzene sulphonamide (Py₁-Ts)

Yield: 88%. M.p: 167−169 °C. FT-IR (ATR), υ_{max} (cm^{-1}): 3383 (N−H), 3068 (ArC−H), 2946−2842 (C−H), 1612 (C=N), 1596 (C=C), 1497−1462 (N–N), 1386, 1345−1158 (SO_2, tosyl), 1042, 1000, 885, 744, 667 (C−S). ^{1}H NMR (400 MHz, δ, ppm, $CDCl_3$): 7.94 (t, 2H, Ar–H), 7.73 (t, 1H, Ar–H), 7.29–7.22 (m, 2H, Ar–H), 7.14 (d, 1H, Ar–H), 7.09 (d, 1H, Ar–H), 7.03 (d, 3H, Ar–H), 6.99 (s, 1H, Ar–H), 6.95 (d, 1H, Ar–H), 6.88–6.83 (m, 1H, Ar–H), 5.51 (t, 1H, pyrazoline –CH), 3.95 (s, 1H, NH), 3.93 (s, 3H, –OCH_3), 3.82 (dd, 1H, pyrazoline –CH_2), 3.01 (dd, 1H, pyrazoline –CH_2), 2.32 (s, 3H, –CH_3). ^{13}C NMR (100 MHz, δ, ppm, $CDCl_3$): 156.0, 148.2, 145.1, 143.6, 143.5, 141.5, 136.7, 136.4, 129.5, 128.9, 128.7, 128.4, 127.4, 126.9, 126.4, 123.9, 123.2, 120.9, 119.8, 113.1, 110.6, 57.2 (pyrazoline –CH), 55.5 (–OCH_3), 42.9 (pyrazoline CH_2), 21.5 (–CH_3). MS (MALDI–TOF) *m/z*: Calculated:497.61; Found:497.45 $[M]^+$.

2.1.2.2. N-(3,4-dicyanophenyl)-N-(3-(5-(2,5-dimethoxyphenyl)-1-phenyl-4,5-dihydro-1H-pyrazol-3-yl) phenyl)-4-methylbenzenesulfonamide (Py₂-Ts)

Yield: 83%. M.p: 157−159 °C. FT-IR (ATR), υ_{max} (cm^{-1}): 3384 (N−H), 3066 (ArC−H), 2949−2838 (C−H), 1660 (C=N), 1596 (C=C), 1497−1455 (N–N), 1386, 1345−1158 (SO_2, tosyl), 1077, 1000, 919, 885, 745, 667 (C−S). ^{1}H NMR (400 MHz, δ, ppm, $CDCl_3$): 7.72 (t, 2H, Ar–H), 7.58 (d, 1H, Ar–H), 7.33–7.22 (m, 2H, Ar–H), 7.14 (d, 1H, Ar–H), 7.09 (d, 1H, Ar–H), 7.05–6.99 (m, 1H, Ar–H), 6.96 (s, 2H, Ar–H), 6.94 (s, 1H, Ar–H), 6.88–6.84 (m, 1H, Ar–H), 5.52 (t, 1H, pyrazoline –CH), 3.98 (s, 1H, NH), 3.93 (s, 6H, –OCH_3), 3.83 (dd, 1H, pyrazoline –CH_2), 3.01 (dd, 1H, pyrazoline –CH_2), 2.32 (s, 3H, –CH_3). ^{13}C NMR (100 MHz, δ, ppm, $CDCl_3$): 156.0, 148.2, 143.6, 143.5, 136.7, 136.4, 130.9, 129.5, 128.9, 128.8, 127.4, 127.2, 127.1, 126.4, 123.2, 122.9, 120.9, 119.8, 113.1, 111.4, 110.6, 57.2 (pyrazoline –CH), 55.5 (–OCH_3), 54.9 (–OCH_3), 42.9 (pyrazoline CH_2), 21.5 (–CH_3). MS (MALDI–TOF) *m/z*: Calculated:527.63; Found:527.67 $[M]^+$.

2.1.3. Methoxylated pyrazoline derivatives bearing nitrile group (Py₁-CN and Py₂-CN)

Py₁-Ts compound (0.5g, 1.0 mmol) or **Py₂-Ts** compound (0.44g, 0.84 mmol) and 4-nitrophthalonitrile (0.17g, 1.0 mmol for **Py₁-CN**) or (0.15g, 0.84 mmol for **Py₂-CN**) were solved in dry dimethylformamide (10 mL). Following thawing, trace amounts of anhydrous K_2CO_3 (0.41g, 3.0 mmol for **Py₁-CN**) or (0.35g, 2.52 mmol for **Py₂-CN**) were added to the reaction mixture. After four days at 55 °C and N_2 atmospheric pressure, the reaction mixture was transferred to ice and filtered. Using silica gel and column chromatography, the obtained solid product was purified. Hereby, the title products (**Py₁-CN** and **Py₂-CN**) were acquired as fawn-colored solids.

2.1.3.1. N-(3,4-dicyanophenyl)-N-(2-(5-(2-methoxyphenyl)-1-phenyl-4,5-dihydro-1H-pyrazol-3-yl) phenyl)-4-methylbenzenesulfonamide (Py₁-CN)

Yield: 48%. Column chromatography solvent: Chloroform. FT–IR (ATR), υ_{max} (cm^{-1}): 3073 (ArC–H), 2922–2836 (C–H), 2233 (C≡N), 1672 (C=N), 1595 (C=C), 1486−1463 (N–N), 1388, 1338−1157 (SO_2, tosyl), 1090, 999, 881, 748, 691 (C−S). ^{1}H NMR (400 MHz, δ, ppm, $CDCl_3$): 7.96 (d, 2H, Ar–H), 7.78 (d, 2H, Ar–H), 7.31–7.28 (m, 2H, Ar–H), 7.18 (d, 2H, Ar–H), 7.11 (d, 2H, Ar–H), 7.00 (d, 2H, Ar–H), 6.97 (s, 1H, Ar–H), 6.93 (d, 1H, Ar–H), 6.87–6.82 (m, 2H, Ar–H), 5.50 (t, 1H, pyrazoline –CH), 3.92 (s, 3H, –OCH_3), 3.80 (dd, 1H, pyrazoline –CH_2), 3.00 (dd, 1H, pyrazoline –CH_2), 2.31 (s, 3H, –CH_3). ^{13}C NMR (100 MHz, δ, ppm, $CDCl_3$): 156.0, 148.2, 143.6, 143.5, 136.7, 136.4, 131.1, 130.9, 129.5, 129.4, 128.9, 128.7, 128.6, 128.4, 128.1, 127.7, 127.4, 126.4, 124.0, 123.2, 122.9, 121.2, 120.9, 120.8, 119.8 (C≡N), 119.1 (C≡N), 113.1, 111.4, 110.6, 107.2, 57.2 (pyrazoline –CH), 55.5 (–OCH_3), (pyrazoline CH_2), 21.5 (–CH_3). MS (MALDI–TOF) *m/z*: Calculated: 623.72; Found: 646.61 $[M+Na]^+$.

2.1.3.2. N-(3,4-dicyanophenyl)-N-(3-(5-(2,5-dimethoxyphenyl)-1-phenyl-4,5-dihydro-1H-pyrazol-3-yl) phenyl)-4-methylbenzenesulfonamide (Py₂-CN)

Yield: 52%. Column chromatography solvent: Chloroform. FT–IR (ATR), υ_{max} (cm^{-1}): 3059 (ArC–H), 2922–2835 (C–H), 2233 (C≡N), 1660 (C=N), 1595 (C=C), 1493−1462 (N–N), 1395, 1328−1158 (SO_2, tosyl), 1091, 999, 875, 747, 691 (C−S). ^{1}H NMR (400 MHz, δ, ppm, $CDCl_3$): 7.78 (t, 2H, Ar–H), 7.62 (m, 2H, Ar–H), 7.47–7.39 (m, 2H, Ar–H), 7.12 (d, 1H, Ar–H), 7.07 (d, 2H, Ar–H), 7.05–6.98 (m, 2H, Ar–H), 6.97 (s, 2H, Ar–H), 6.92 (s, 1H, Ar–H), 6.88–6.84 (m, 1H, Ar–H), 5.51 (t, 1H, pyrazoline –CH), 3.95 (s, 6H, –OCH_3), 3.85 (dd, 1H, pyrazoline –CH_2), 3.03 (dd, 1H, pyrazoline –CH_2), 2.30 (s, 3H, –CH_3). ^{13}C NMR (100 MHz, δ, ppm, $CDCl_3$): 156.0, 148.3, 143.7, 143.5, 137.7, 136.4, 135.6, 134.7, 132.9, 130.9, 129.5, 129.2, 128.9, 128.1, 127.9, 127.4, 127.2, 127.1, 126.4, 123.2, 122.9, 121.6,

120.9, 120.8, 119.8 (C≡N), 119.1 (C≡N), 113.1, 111.4, 110.6, 57.2 (pyrazoline –CH), 55.5 (–OCH_3), 54.9 (–OCH_3), 42.9 (pyrazoline CH_2), 21.5 (–CH_3). MS (MALDI–TOF) *m/z*: Calculated: 653.75; Found: 676.67 $[M+Na]^+$.

2.2. Theoretical methods

Theoretical computations can teach us a great deal about the chemical and biological properties of molecules. Many properties of quantum chemicals are determined by theoretical calculations (Tas et. al. 2022). The chemical behavior of the molecules is explained by the estimated parameters. Numerous programs are used to calculate molecules. Gaussian09 RevD.01 and GaussView 6.0 (Dennington et. al. 2016; Frisch et. al. 2009) are the programs in question. These programs were used to do calculations utilizing the 6-31++g(d,p) basis set using the B3LYP, HF, and M06-2x (Becke 1992), (Hohenstein et. al. 2008), (Vautherin and Brink 1972) methods. The outcome of these efforts has been the discovery of numerous quantum chemical parameters. The estimated parameters are calculated as follows, where each parameter describes a different chemical characteristic of molecules (Lakhrissi et. al. 2022; Majumdar et. al. 2022).

$$\chi = -\left(\frac{\partial \mathrm{E}}{\partial \mathrm{N}}\right)_{v(r)} = \frac{1}{2}(I + A) \cong -\frac{1}{2}(E_{HOMO} + E_{LUMO})$$

$$\eta = -\left(\frac{\partial^2 \mathrm{E}}{\partial \mathrm{N}^2}\right)_{v(r)} = \frac{1}{2}(I - A) \cong -\frac{1}{2}(E_{HOMO} - E_{LUMO})$$

$$\sigma = 1/\eta \qquad \omega = \chi^2/2\eta \qquad \varepsilon = 1/\omega$$

Molecular docking calculations are performed to compare the biological activity of a molecule to that of a biological substance. Schrödinger's Maestro Molecular Modeling Platform (version 12.8a) was used to do the molecular docking computations (Schrödinger 2021-3; 2021). There are several steps involved in computation. Each step is completed in a different way. In the first phase, proteins were prepared using the protein preparation module (Schrödinger 2019-4; 2016; 2019). In this module, the protein active sites were found. After then, computations using optimized structures can be performed with the LigPrep module (Schrödinger 2021-3; 2021). Following preparation, the Glide ligand docking module was used to examine the interactions between the compounds and the cancer protein (Tüzün et. al. 2022). Every calculation was carried out with the OPLS4 technique. To evaluate the chemicals under investigation's pharmacological potential, an ADME/T (absorption, distribution, metabolism, excretion, and toxicity) study was conducted. The Qik-prop module of the Schrödinger software (Schrödinger 2021-3; 2021) was used to predict the results and interactions of molecules involved in human metabolism.

3. Results and Discussion

3.1. Characterizations of synthesized all compounds

General synthesis schemes of methoxylated pyrazoline derivatives bearing amine (**Py_1-NH_2** and **Py_2-NH_2**), tosyl (**Py_1-Ts** and **Py_2-Ts**), and nitrile (**Py_1-CN** and **Py_2-CN**) groups are given in Schemes 1 and 2.

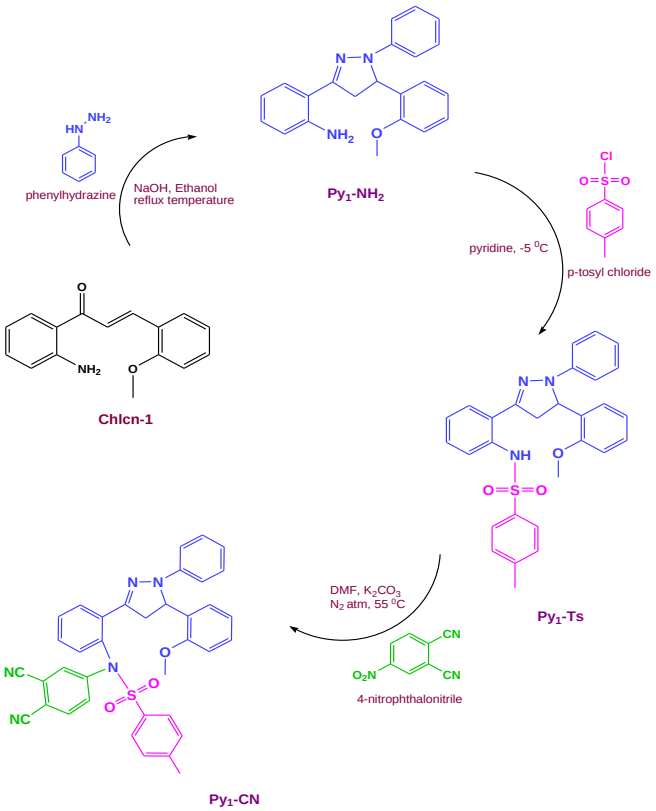

Scheme 1. Synthesis scheme of methoxylated pyrazoline derivatives bearing amine (Py_1-NH_2), tosyl (Py_1-Ts), and nitrile (Py_1-CN) groups.

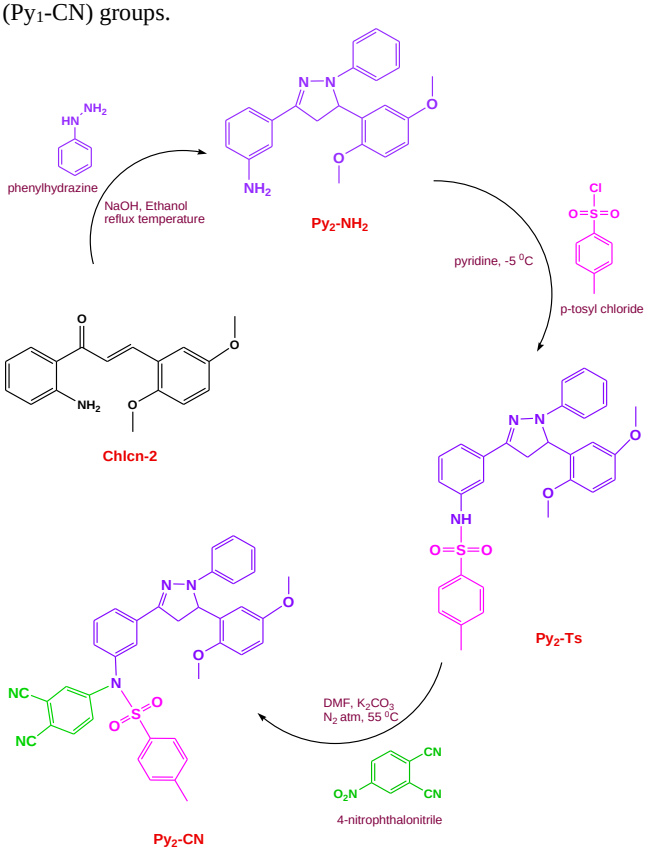

Scheme 2. Synthesis scheme of methoxylated pyrazoline derivatives bearing amine (**Py_2-NH_2**), tosyl (**Py_2-Ts**), and nitrile (**Py_2-CN**) groups.

These compounds' structural characterizations were carried out with the use of mass, FT-IR, and NMR spectrum data. Attained methoxylated pyrazoline derivatives bearing amine (**Py_1-NH_2** and **Py_2-NH_2**) groups have characteristic groups of NH_2 (amine), C=N (due to ring closure), and N–N (proves the formation of a pyrazoline ring). NH_2 stretching vibration was seen at 3384−3291 cm^{-1} (for **Py_1-NH_2**) and 3443−3361 cm^{-1} (for **Py_2-NH_2**), C=N stretching vibration was seen at 1615 cm^{-1} (for **Py_1-NH_2**) and 1618 cm^{-1} (for **Py_2-NH_2**), and N–N stretching vibration was seen at 1492−1446 cm^{-1} (for **Py_1-NH_2**) and 1495−1462 cm^{-1} (for **Py_2-NH_2**) in the FT-IR spectra. NMR spectra of methoxylated pyrazoline derivatives bearing amine (**Py_1-NH_2** and **Py_2-NH_2**) groups were recorded in DMSO-d_6 (Fig.2). The mass spectra of **Py_1-NH_2** and **Py_2-NH_2** showed two distinct molecular ion peaks, located at m/z: 343.51 $[M]^+$ and 373.76 $[M]^+$, respectively (Fig. 3). The data obtained proves the formation of methoxylated pyrazoline derivatives bearing an amine group.

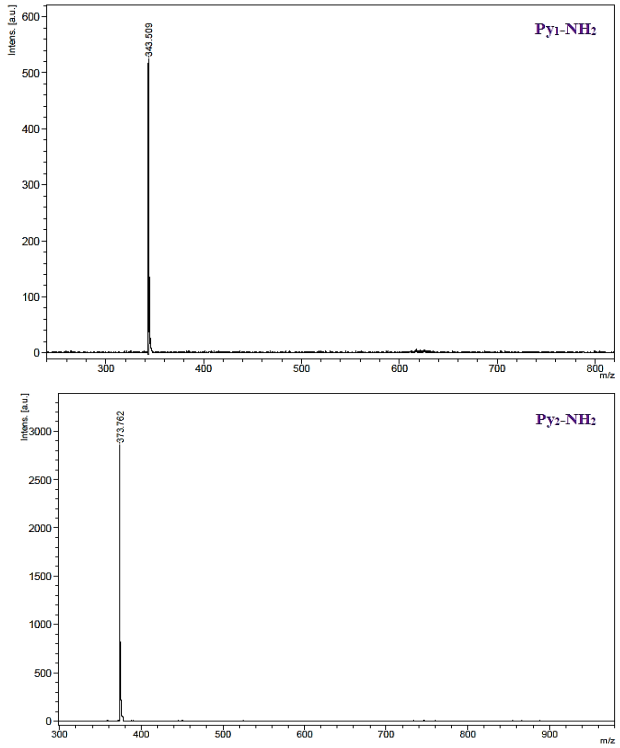

Fig. 2. Mass spectra of pyrazoline derivatives bearing the amine (**Py_1/Py_2-NH_2**) group.

Obtained methoxylated pyrazoline derivatives bearing tosyl (**Py_1-Ts** and **Py_2-Ts**) group have characteristic groups as N−H, C=N (due to ring closure), N–N (proves the formation of pyrazoline ring), and SO_2 (tosyl). The FT-IR spectra showed the following: N-H stretching vibration was observed at 3383 cm^{-1} (for **Py_1-Ts**) and 3384 cm^{-1} (for **Py_2-Ts**); C=N stretching vibration was observed at 1612 cm^{-1} (for **Py_1-Ts**) and 1660 cm^{-1} (for **Py_2-Ts**); N-N stretching vibration was observed at 1497−1462 cm^{-1} (for **Py_1-Ts**) and 1497−1455 cm^{-1} (for **Py_2-Ts**); and SO_2 (tosyl) stretching vibration was observed at 1345−1158 cm^{-1} (for **Py_1/Py_2-Ts**). Methoxylated pyrazoline derivatives with tosyl groups (**Py_1-Ts** and **Py_2-Ts**) were recorded in $CDCl_3$ and their NMR spectra were obtained. Doublet of doublet (dd) characteristic peaks were observed in the ^1H NMR spectra at 3.82 and 3.01 ppm (for **Py_1-Ts**), and 3.83 ppm and 3.01 ppm (for **Py_2-Ts**). Additionally, for **Py_1-Ts** and **Py_2-Ts**, aromatic protons were detected at 7.94–6.83 ppm and 7.72–6.84 ppm, respectively. The molecular ion peak for **Py_1-Ts** and **Py_2-Ts**, respectively, were found in the mass spectra at m/z: 497.45 $[M]^+$ and 527.67 $[M]^+$, as shown in Figure 4. The information gathered demonstrates the creation of derivatives of methoxylated pyrazolines with a tosyl group.

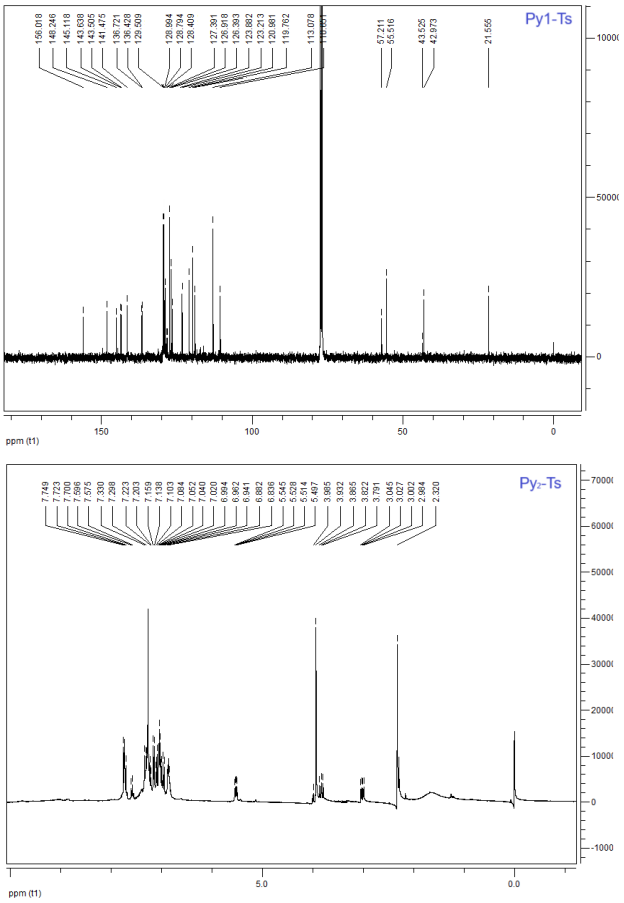

Fig. 2. ^{13}C NMR and ^1H NMR spectra of pyrazoline derivatives bearing the tosyl (**Py_1/Py_2-Ts**) group.

The distinctive groups of methylated pyrazoline derivatives with nitrile groups (**Py_1-CN** and **Py_2-CN**) are C≡N (nitrile), C=N (because of ring closure), N-N (shows that the pyrazoline ring is formed), and SO_2 (tosyl). In the FT-IR spectra, several stretching vibrations were observed: C≡N was observed at 2233 cm^{-1} (for **Py_1/Py_2-CN**), C=N was observed at 1672 cm^{-1} (for **Py_1-CN**) and 1660 cm^{-1} (for **Py_2-CN**), N-N was observed at 1486−1463 cm^{-1} (for **Py_1-CN**) and 1493−1462 cm^{-1} (for **Py_2-CN**), and SO_2 (tosyl) was observed at 1338−1157 cm^{-1} (for **Py_1-CN**) and 1328−1158 cm^{-1} (for **Py_2-CN**). Methoxylated pyrazoline derivatives (**Py_1-CN** and **Py_2-CN**) with nitrile groups recorded their NMR spectra in $CDCl_3$. A molecular ion peak for **Py_1-CN** and **Py_2-CN**, respectively, was seen in the mass spectra at m/z: 646.61 $[M+Na]^+$ and 676.67 $[M+Na]^+$, respectively. The information gathered demonstrates the creation of derivatives of methoxylated pyrazolines with a nitrile group.

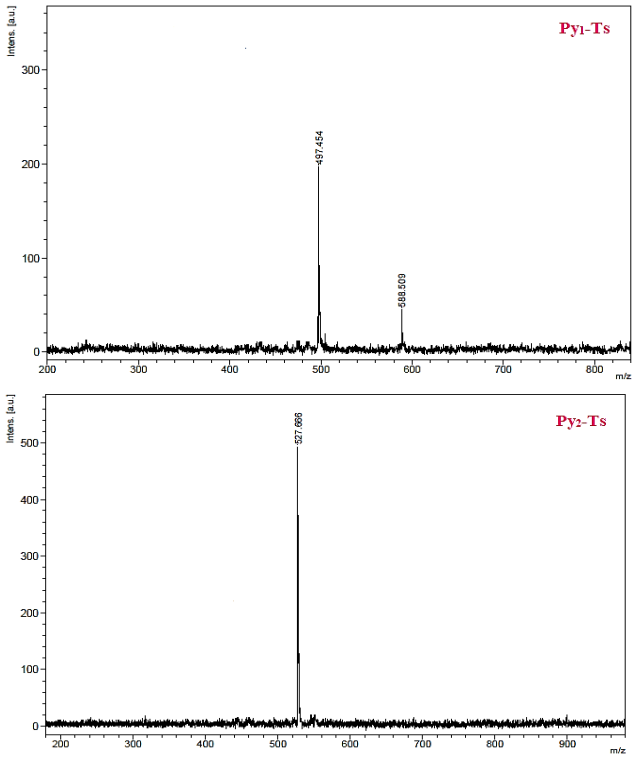

Fig. 4. Mass spectra of pyrazoline derivatives bearing the tosyl (**Py1**/**Py2-Ts**) group.

3.2. Theoretical calculations

One popular technique for comparing the activity of molecules is to perform theoretical calculations. This approach provides significant insights into the molecular features that are both chemical and biological. For this data, numerous parameters are determined (Majumdar et. al. 2022). A distinct piece of information about the molecule is provided by each parameter. The Gaussian software program is used to calculate a number of quantum chemical parameters, the numerical values of which are utilized to explain the behaviors of molecules. The HOMO and LUMO parameters are more significant than the other estimated values for the molecules. The molecule with the greatest HOMO parameter numerical value is assumed to have higher activity than the other molecules since it can donate electrons more readily than the others (Majumdar et. al. 2022). LUMO is an additional parameter. It is believed that the molecule with the lowest numerical expression of this characteristic has a higher activity than the other molecules because it can acquire electrons more readily than the other molecules (Lakhrissi et. al. 2022). The ΔE energy gap is the next parameter, and for highly active molecules, its numerical expression is the smallest. The electronegativity value reveals how well-suited the molecules' atoms are to luring bind electrons (Majumdar. et al. 2022). More electrons are drawn to molecules with higher electronegativity. The activity in this instance declines. Gaussian calculations yielded numerous parameters, which are included in Table 1.

When the HOMO energy values in this table are examined, it is seen that **Py1-NH2** has higher activity than other molecules as a result of the calculations made in the B3LYP and M062X methods. Another parameter is the LUMO parameter; according to this parameter, **Py1-CN** was found to have higher activity than other molecules. Another important parameter used to compare the activities of molecules is electronegativity, which has a lower electronegativity for **Py2-NH2**. For this reason, it is seen that its activity is higher since it will interact by giving electrons more easily (Fig. 5).

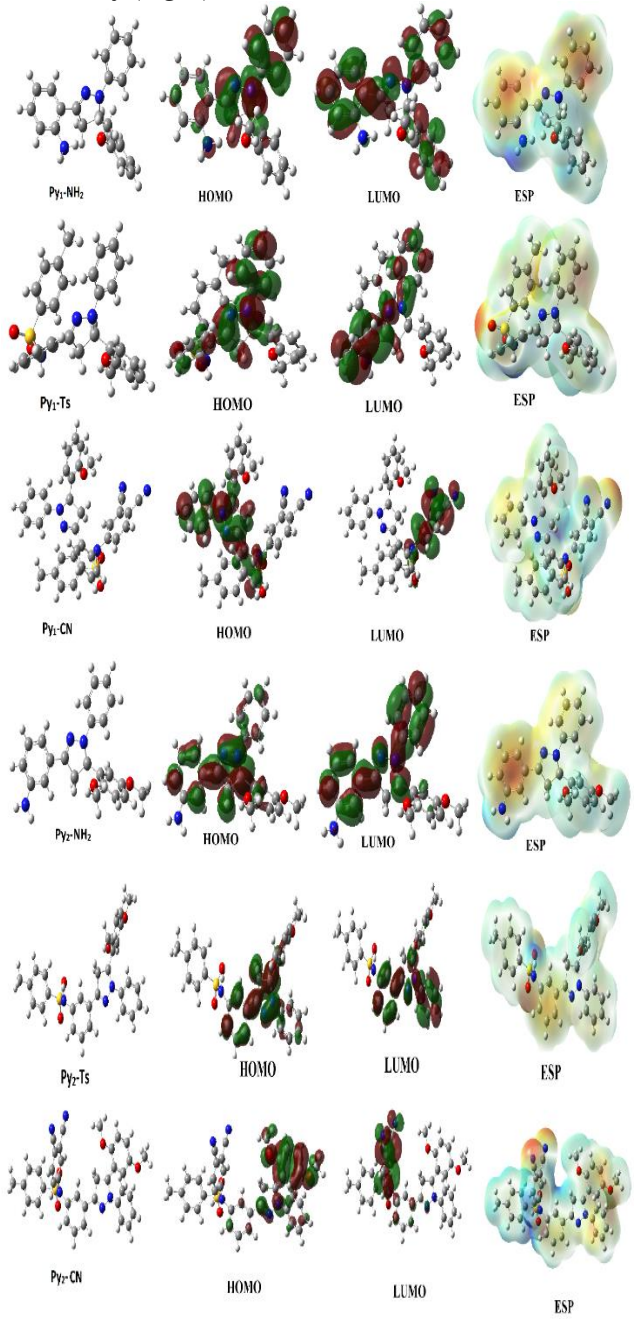

Fig. 5. Representations of molecules' ESP, HOMO, LUMO, and optimal structures.

Gaussian calculations are essential to elucidate the chemical properties of molecules. To further evaluate the biological activity of these molecules, another important calculation is required: molecular docking. Molecular docking studies evaluate the interactions between molecules and biological targets, usually proteins associated with human cancer cells.

This approach provides a detailed insight into how the molecule under study interacts with cancer cell proteins. The interactions include various forces such as chemical bonding, hydrogen bonding, polar and hydrophobic contacts, as well as π-π and halogen interactions (Çelik et al., 2023; Tapera et al., 2022). Figures 6-9 show these molecular interactions in detail.

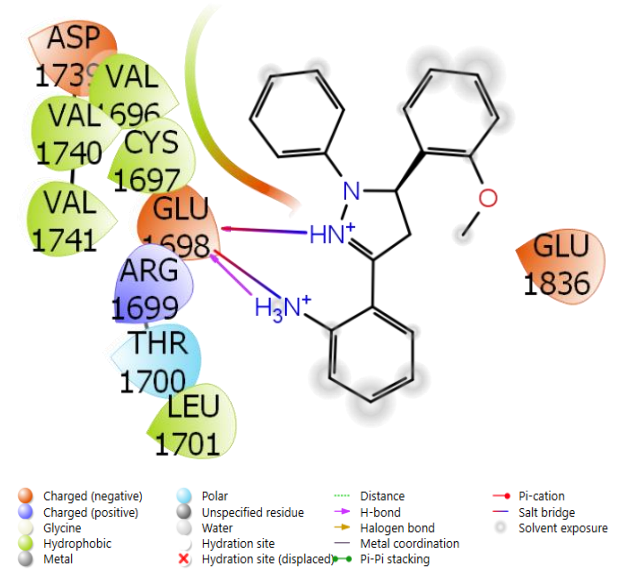

Fig. 6. Presentation interactions of **Py_1-NH_2** with Breast cancer

As a result of the docking calculations, when the interactions that occur between molecules and proteins are examined, in Figure 6, when the interactions that occur between **Py_1-NH_2** and Breast cancer are examined, it is seen that there is a salt bridge interaction between the nitrogen atom in the pyrazole ring of the **Py_1-NH_2** molecule and the GLU 1698 protein. In addition, it is seen that the nitrogen and hydrogen atom in the aniline ring of the **Py_1-NH_2** molecule make hydrogen bonds with the GLU 1698 protein. When the interactions between **Py_1-NH_2** and Prostate cancer are examined in figure 7, it is seen that there is a hydrogen bond interaction between the nitrogen atom in the pyrazole ring and the TRP 114 protein. When the interactions between **Py_1-NH_2** and Colon cancer are examined in figure 8, it is seen that there is a salt bridge interaction between the nitrogen atom in the pyrazole ring of the **Py_1-NH_2** molecule and the GLU 885 and ASP 1046 proteins. In addition, it is seen that there is a salt bridge interaction between the nitrogen atom in the aniline ring attached to the central ring of the **Py_1-NH_2** molecule and the GLU 885 and ASP 1046 proteins. When the interactions between **Py_2-Ts** and Liver cancer are examined in Figure 9, it is seen that a π-π interaction occurs between the benzene ring attached to the pyrazole ring in the **Py2-Ts** molecule and the PHE 135 protein. It is seen that a π-π interaction occurs between the toluene ring in the **Py_2-Ts** molecule and the TRP 296 protein. It is seen that the nitrogen atom attached to the sulfur dioxide group in the **Py_2-Ts** molecule forms a salt bridge with the Mg1440 and Mg 1439 atoms.

The results obtained from the calculations made are given in Table 2. The most important of these parameters is the Docking Score parameter, which gives the numerical value of the chemical interactions between molecules and proteins. It is assumed that the molecule with the greatest negative numerical value of this parameter has more chemical interactions since its activity is greater than that of other molecules (Çelik et. al. 2023). It should be common knowledge that when the molecule and protein interact more, the docking score parameter rises and therefore does the molecule's activity.

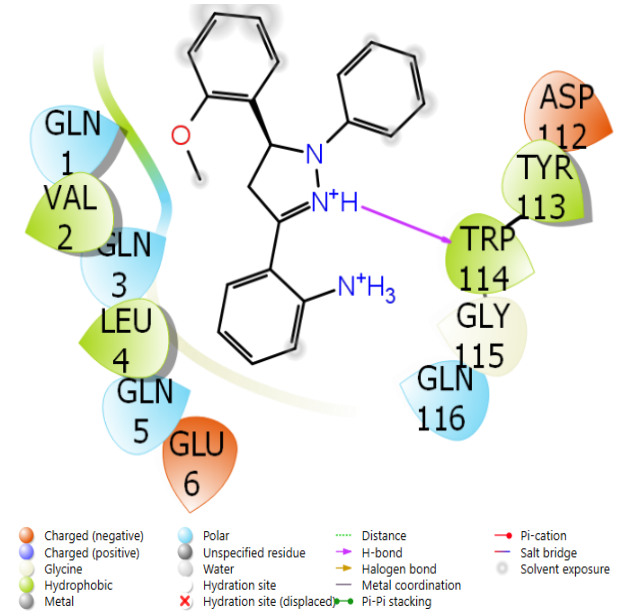

Fig. 7. Presentation interactions of **Py_1-NH_2** with Prostate cancer

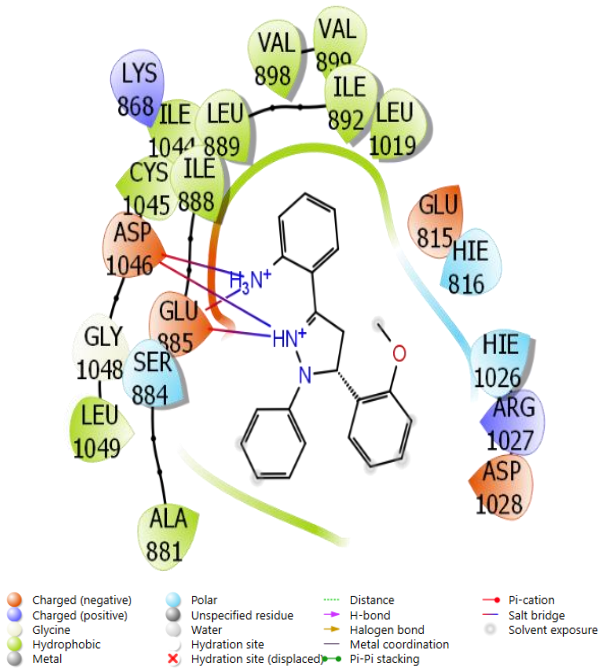

Fig. 8. Presentation interactions of **Py$_1$-NH$_2$** with Colon cancer

Glide ligand efficiency, glide hbond, glide evdw, and glide ecoul are additional factors in the docking computations that provide a numerical value for the chemical interactions between chemicals and proteins (Çelik et. al. 2023). Additional determined parameters include a pose resulting from the interaction of molecules with proteins; Glide emodel, Glide energy, Glide internal, and Glide posenum are the essential factors that provide numerical values for this pose (Tüzün et. al. 2022).

Comparing the activities of the studied molecules with molecular docking calculations is not sufficient by itself for the molecules to be used in human metabolism. Even if the molecules have high activity against cancer proteins, it does not allow us to comment on how they will act in human metabolism. For this, it is necessary to examine the ADME properties of molecules (Table 3).

As a result of this theoretical analysis, many parameters were obtained and these parameters are given in Table 3. The first parameter among these parameters is Solute Molecular Weight, which requires the molecule to have a certain molecular weight.

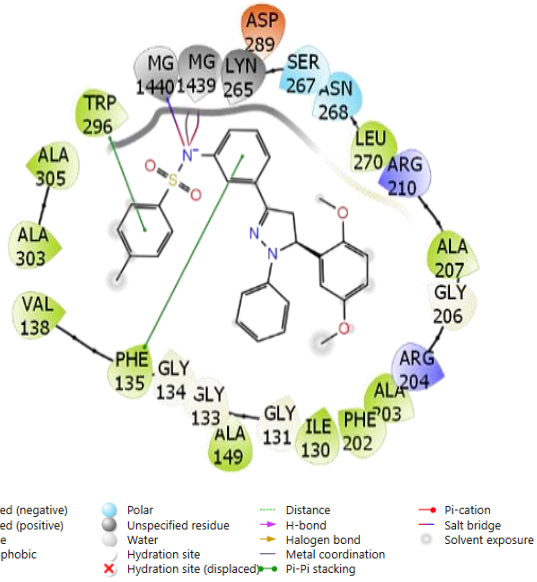

Fig. 9. Presentation interactions of **Py$_2$-Ts** with Liver cancer

Another parameter is PISA, which is also called Solute Total SASA. This parameter is π (carbon and attached hydrogen) component of the SASA. Another parameter is QP Polarizability, which is the parameter that predicted polarizability in cubic angstroms.

Another important parameter is QPlogHERG, which is the numerical value of the estimated IC_{50} value when the HERG K channels are blocked. The next parameter is QPPCaco, which is the Caco-2 cell permeability in the intestinal-blood barrier for inactive transport. Another parameter is QPlogBB, which is the brain-blood barrier coefficient of an orally administered drug. The next parameter is Human Oral Absorption, which predicts qualitative human oral absorption: 1, 2, or 3 for low, medium, or high.

It enables the examination of many properties of molecules, such as absorption by human metabolism, movements, and excretion by human metabolism. In ADME analysis, many biological and chemical properties of molecules are examined. At the beginning of these, many properties of molecules, such as molecular masses, dipole moments,

Table 1. The calculated quantum chemical parameters of molecules.

	E_{HOMO}	E_{LUMO}	I	A	ΔE	η	μ	χ	Pİ	ω	ε	dipol	Energy
B3LYP/6-31++g(d,p)LEVEL													
Py_1-NH_2	-5.8091	-4.9650	5.8091	4.9650	0.8441	0.4221	2.3694	5.3871	-5.3871	34.3804	0.0291	4.0298	-29665.2437
Py_1-Ts	-5.2654	-1.5663	5.2654	1.5663	3.6991	1.8496	0.5407	3.4159	-3.4159	3.1543	0.3170	4.4593	-51947.6386
Py_1-CN	-3.7283	-2.3644	3.7283	2.3644	1.3638	0.6819	1.4664	3.0463	-3.0463	6.8044	0.1470	4.9789	-63236.1369
Py_2-NH_2	-3.8951	-1.2828	3.8951	1.2828	2.6123	1.3062	0.7656	2.5889	-2.5889	2.5657	0.3898	4.4165	-32764.1339
Py_2-Ts	-3.9715	-1.5037	3.9715	1.5037	2.4678	1.2339	0.8104	2.7376	-2.7376	3.0369	0.3293	7.1815	-55046.4392
Py_2-CN	-4.1481	-2.4436	4.1481	2.4436	1.7045	0.8523	1.1733	3.2959	-3.2959	6.3729	0.1569	4.7346	-66352.1260
HF/6-31++g(d,p)LEVEL													
Py_1-NH_2	-7.4274	0.9878	7.4274	-0.9878	8.4152	4.2076	0.2377	3.2198	-3.2198	1.2320	0.8117	2.5881	-29475.6565
Py_1-Ts	-7.5888	0.8958	7.5888	-0.8958	8.4846	4.2423	0.2357	3.3465	-3.3465	1.3199	0.7576	4.2304	-51670.7547
Py_1-CN	-7.7254	0.7908	7.7254	-0.7908	8.5161	4.2581	0.2348	3.4673	-3.4673	1.4117	0.7084	8.7016	-62907.1335
Py_2-NH_2	-6.8571	0.9521	6.8571	-0.9521	7.8092	3.9046	0.2561	2.9525	-2.9525	1.1163	0.8959	4.8993	-32557.4449
Py_2-Ts	-6.9428	0.9236	6.9428	-0.9236	7.8663	3.9332	0.2542	3.0096	-3.0096	1.1515	0.8685	7.6145	-54752.4914
Py_2-CN	-6.9373	0.6667	6.9373	-0.6667	7.6040	3.8020	0.2630	3.1353	-3.1353	1.2928	0.7735	5.3347	-65989.6125
M062X/6-31++g(d,p)LEVEL													
Py_1-NH_2	-6.2842	-0.2267	6.2842	0.2267	6.0576	3.0288	0.3302	3.2555	-3.2555	1.7495	0.5716	2.9974	-29652.5460
Py_1-Ts	-6.5468	-0.6248	6.5468	0.6248	5.9221	2.9610	0.3377	3.5858	-3.5858	2.1712	0.4606	4.0107	-51929.3708
Py_1-CN	-6.8426	-1.4836	6.8426	1.4836	5.3591	2.6795	0.3732	4.1631	-4.1631	3.2340	0.3092	8.3285	-63230.9218
Py_2-NH_2	-4.8107	-0.4150	4.8107	0.4150	4.3958	2.1979	0.4550	2.6129	-2.6129	1.5531	0.6439	2.5039	-32749.9429
Py_2-Ts	-4.9604	-0.6280	4.9604	0.6280	4.3324	2.1662	0.4616	2.7942	-2.7942	1.8022	0.5549	7.0935	-55026.5510
Py_2-CN	-6.8426	-1.4836	6.8426	1.4836	5.3591	2.6795	0.3732	4.1631	-4.1631	3.2340	0.3092	8.3285	-63230.9217

Table 2. The docking parameters of molecules against enzymes are expressed numerically

1JNX	Docking Score	Glide ligand efficiency	Glide hbond	Glide evdw	Glide ecoul	Glide emodel	Glide energy	Glide einternal	Glide posenum
Py_1-NH_2	-4.29	-0.17	-0.40	-22.00	-12.02	-44.32	-34.02	3.03	45
Py_1-Ts	-3.76	-0.10	-0.16	-26.68	-14.01	-50.70	-40.69	4.54	6
Py_1-CN	-2.79	-0.06	0.00	-38.94	-1.57	-44.44	-40.51	1.03	216
Py_2-NH_2	-3.54	-0.13	-0.55	-26.10	-4.58	-36.01	-30.68	3.89	44
Py_2-Ts	-2.76	-0.07	-0.32	-32.78	-4.13	-43.74	-36.91	0.96	343
Py_2-CN	-3.33	-0.07	-0.27	-32.77	-6.95	-47.39	-39.72	2.04	180
6XXP	Docking Score	Glide ligand efficiency	Glide hbond	Glide evdw	Glide ecoul	Glide emodel	Glide energy	Glide einternal	Glide posenum
Py_1-NH_2	-4.79	-0.18	0.00	-27.49	-8.00	-45.23	-35.49	2.79	67
Py_1-Ts	-3.54	-0.10	0.00	-31.76	-7.42	-46.22	-39.18	3.97	337
Py_1-CN	-1.39	-0.03	0.00	-28.20	-0.52	-27.26	-28.72	4.45	262
Py_2-NH_2	-	-	-	-	-	-	-	-	-
Py_2-Ts	-2.67	-0.07	-0.50	-25.17	-8.38	-37.48	-33.54	2.11	174
Py_2-CN	-2.56	-0.05	0.00	-29.58	-6.42	-38.58	-36.00	2.53	366
3WZE	Docking Score	Glide ligand efficiency	Glide hbond	Glide evdw	Glide ecoul	Glide emodel	Glide energy	Glide einternal	Glide posenum
Py_1-NH_2	-6.08	-0.23	-0.01	-36.39	-5.32	-61.46	-41.71	0.76	234
Py_1-Ts	-5.57	-0.15	-0.16	-33.54	-3.67	-45.73	-37.22	5.17	47
Py_1-CN	-4.20	-0.09	0.00	-17.32	0.73	-31.08	-16.59	19.02	86
Py_2-NH_2	-6.01	-0.21	-0.27	-41.31	-1.96	-56.10	-43.27	8.06	295
Py_2-Ts	-4.15	-0.11	0.00	-51.45	0.76	-56.45	-50.69	8.25	49
Py_2-CN	-	-	-	-	-	-	-	-	-
4UYA	Docking Score	Glide ligand efficiency	Glide hbond	Glide evdw	Glide ecoul	Glide emodel	Glide energy	Glide einternal	Glide posenum
Py_1-NH_2	-4.60	-0.18	0.00	-28.94	-0.60	-34.29	-29.54	1.35	393
Py_1-Ts	-5.38	-0.15	0.00	-46.10	-1.61	-51.33	-47.71	11.66	89
Py_1-CN	-5.97	-0.13	-0.32	-52.32	-3.70	-73.12	-56.01	9.78	124
Py_2-NH_2	-5.63	-0.20	-0.32	-37.81	-4.28	-54.55	-42.09	4.66	359
Py_2-Ts	-7.94	-0.21	-0.16	-44.83	-14.87	-112.10	-59.70	5.20	68
Py_2-CN	-5.50	-0.11	-0.06	-47.84	-5.30	-68.06	-53.14	14.93	279

Table 3. ADME properties of molecule

	Py_1-NH_2	**Py_1-Ts**	**P_1y-CN**	**Py_2-NH_2**	**Py_2-Ts**	**Py_2-CN**	**Referance Range**
mol_MW	343	343	343	343	343	343	130-725
dipole (D)	3.0	7.4	10.6	5.3	8.0	4.7	1.0-12.5
SASA	632	759	871	671	883	1051	300-1000
FOSA	100	198	135	211	298	332	0-750
FISA	44	74	170	68	80	196	7-330
PISA	487	486	567	392	505	522	0-450
WPSA	0.0	0.0	0.5	0.0	0.4	0.6	0-175
volume (A^3)	1129	1468	1776	1215	1621	1970	500-2000
donorHB	1.5	1	0	1.5	1	0	0-6
accptHB	2.75	6.25	9.25	3.5	7	10	2.0-20.0
glob (Sphere =1)	0.8	0.8	0.8	0.8	0.8	0.7	0.75-0.95
QPpolrz (A^3)	42.4	54.7	65.8	44.3	60.3	72.5	13.0-70.0
QPlogPC16	12.8	16.0	19.7	13.1	17.9	22.3	4.0-18.0
QPlogPoct	17.8	23.9	28.9	19.0	26.0	30.5	8.0-35.0
QPlogPw	9.3	12.1	14.4	9.4	13.1	15.2	4.0-45.0
QPlogPo/w	5.4	5.9	5.9	5.3	6.6	6.5	-2.0-6.5
QPlogS	-6.4	-7.1	-7.7	-6.6	-8.9	-10.6	-6.5-0.5
CIQPlogS	-6.3	-8.5	-11.0	-6.6	-8.8	-11.3	-6.5-0.5
QPlogHERG	-6.6	-6.7	-7.2	-6.3	-7.9	-8.5	*
QPPCaco (nm/sec)	3757	1966	245	2256	1744	137	**
QPlogBB	0.0	-0.4	-1.6	-0.3	-0.7	-2.4	-3.0-1.2
QPPMDCK (nm/sec)	2068	1028	109	1192	907	58	**
QPlogKp	-0.4	-0.8	-2.0	-1.1	-0.7	-2.5	Kp in cm/hr
IP (ev)	8.5	8.9	8.5	8.1	8.1	7.1	7.9-10.5
EA (eV)	-0.2	0.6	1.0	0.1	0.6	1.3	-0.9-1.7
#metab	6	6	6	7	7	7	1-8
QPlogKhsa	1.0	1.2	1.0	1.1	1.4	1.3	-1.5-1.5
Human Oral Absorption	1	1	1	1	1	1	-
Percent Human Oral Absorption.	100	100	78.133	100	100	78	***
PSA	45	74	99	54	76	112	7-200
RuleOfFive	1	1	2	1	2	2	Maximum is 4
RuleOfThree	1	1	1	2	2	2	Maximum is 3
Jm	0.1	0.0	0.0	0.0	0.0	0.0	-

*corcern below -5, **<25 is poor and >500 is great, *** <25% is poor and >80% is high.

volume, and the number of hydrogen bonds occurring between a molecule and a protein, are considered chemical properties (Tüzün et. al. 2022). In addition, many biological properties of molecules, such as blood-intestinal barrier and blood-brain barrier transitions in human metabolism, absorption by the skin, and orally usable properties, were investigated. In addition to these properties, the numerical values of the molecules RuleOfFive (Lipinski 2004), (Lipinski et. al. 1997), violations of Lipinski's rule of five, and RuleOfThree (Jorgensen and Duffy 2002), violations of Jorgensen's rule of three, are checked. The numerical value of these two parameters is expected to be zero, but within the desired confidence interval. On the other hand, the numerical values of the QPPCaco (nm/sec) and QPPMDCK (nm/sec) parameters were found to be quite high for some molecules. For this reason, it is thought that it may be a drug for different regions of human metabolism.

5. Conclusion

In the present study, in silico studies of synthesized methoxylated pyrazoline derivatives bearing amine (**Py_1-NH_2** and **Py_2-NH_2**), tosyl (**Py_1-Ts** and **Py_2-Ts**), and nitrile (**Py_1-CN** and **Py_2-CN**) groups were researched. The activities of the molecules were compared as a result of the theoretical calculations. The **Py_1-NH_2** molecule was shown to be usually more active than other compounds in the Gaussian calculations. But when the compounds' actions against cancer proteins were investigated following the molecular docking computations, it was found that, overall, the **Py_1-NH_2** molecule had more activity than the others. As a result of the calculations, the activities of the molecules were compared with the docking calculations. As a result of the calculations, the activities of the molecules were compared with the docking calculations. The **Py_1-NH_2** molecule was generally the most active molecule. It was observed that the **Py_1-NH_2** molecule had the highest activity against the 1JNX protein with a docking score value of -4.29, the **Py_1-NH_2** molecule had the highest activity against the 6XXP protein with a docking score value of -4.79, and the **Py_1-NH_2** molecule had the highest activity against the 3WZE protein with a docking score value of -6.08. In addition, the **Py_2-Ts** molecule had the highest activity against the 4UYA protein with a docking score value of -7.94. After a thorough analysis of the compounds' interactions with cancer proteins, the molecules' ADME characteristics were investigated. This investigation revealed that employing the compounds as medications for human metabolism would not be harmful.

Acknowledgements

The numerical calculations reported in this paper were fully/partially performed at TUBITAK ULAKBIM, High Performance and Grid Computing Center (TRUBA resources). This work was supported by the Scientific Research Project Fund of Sivas Cumhuriyet University (CUBAP) under the project number RGD-020.

Authors' contributions:

HY: Conceptualization, Validation, Methodology, Investigation, Writing-Original Draft, Writing-Review&Editing, Visualization.
DK: Conceptualization, Validation, Methodology, Investigation.
SF: Conceptualization, Validation, Methodology, Investigation.
BT: Funding acquisition, Methodology, Resources, Validation, Visualization, Writing-Original Draft,Writing-Review&Editing.
HK: Funding acquisition, Methodology, Resources, Validation, Visualization, Writing-Review&Editing.

Conflict of interest disclosure:

The authors declare no conflict of interest.

References

Ahmed NM, Youns M, Soltan MK, Said AM. 2019. Design, synthesis, molecular modelling, and biological evaluation of novel substituted pyrimidine derivatives as potential anticancer agents for hepatocellular carcinoma. J Enzym Inhib Med Chem. 34:1110−1120.

Altintop MD, Özdemir A, Kaplancikli ZA, Turan-Zitouni G, Temel HE, Çiftçi GA. 2013. Synthesis and biological evaluation of some pyrazoline derivatives bearing a dithiocarbamate moiety as new cholinesterase inhibitors. Arch Pharmazie. 346: 189−199.

Amr AEGE, El-Naggar M, Al-Omar MA, Elsayed EA, Abdalla MM. 2018. In vitro and in vivo anti-breast cancer activities of some synthesized pyrazolinylestran-17-one candidates. Molecules. 23:1572.

Becke AD. 1992. Density-functional thermochemistry. I. The effect of the exchange-only gradient correction. J Chem Phys. 96(3):2155–2160.

Bhutani R, Pathak DP, Husain A, Kapoor G, Kant R. 2015. A review on recent development of pyrazoline as a pharmocologically active molecule, Int J Pharma Sci Res. 6: 4113−4128.

Chalkha M, el Hassani AA, Nakkabi A, Tüzün B, Bakhouch M, Benjelloun AT, Sfaira M, Saadi M, El Ammari L, El Yazidi M. 2023. Crystal structure, Hirshfeld surface and DFT computations, along with molecular docking investigations of a new pyrazole as a tyrosine kinase inhibitör. J Mol Struct. 1273:134255.

Chen V, Zhang YL, Fan J, Ma X, Qin YJ, Zhu HL. 2018. Novel nicotinoyl pyrazoline derivates bearing N-methyl indole moiety as antitumour agents: design, synthesis and evaluation, Eur J Med Chem. 156:722−737.

Çelik G, Arslan T, Şentürk M, Ekinci D. 2020. Synthesis and characterization of some new pyrazolines and their inhibitory potencies against carbonic anhydrases. Arch Pharmazie. 353:1900292.

Çelik MS, Çetinus ŞA, Yenidünya AF, Çetinkaya S, Tüzün B. 2023. Biosorption of Rhodamine B dye from aqueous solution by Rhus coriaria L. plant: Equilibrium, kinetic, thermodynamic and DFT calculations. J Mol Struct. 1272:134158.

Dennington R, Keith TA, Millam JM. 2016. GaussView 6.0. 16. Semichem Inc.: Shawnee Mission, KS, USA.

Dipankar B, Hirakmoy C, Asish B, Abhijit C. 2011. 2-pyrazoline: a pharmacologically active moiety. Int Res J Pharmaceut Appl Sci. 1:68−80.

Frisch MJ, Trucks GW, Schlegel HB, Scuseria GE, Robb MA, Cheeseman JR, Scalmani G, Barone V, Mennucci B, Petersson GA, Nakatsuji H, Caricato M, Li X, Hratchian HP, Izmaylov AF, Bloino J, Zheng G, Sonnenberg JL, Hada M, Ehara M, Toyota K, Fukuda R, Hasegawa J, Ishida M, Nakajima T, Honda Y, Kitao O, Nakai H, Vreven T, Montgomery JA, Peralta JE, Ogliaro F, Bearpark M, Heyd JJ, Brothers E, Kudin KN, Staroverov VN, Kobayashi R, Normand J, Raghavachari K, Raghavachari AR, Burant JC, Iyengar SS, Tomasi J, Cossi M, Rega N, Millam JM, Klene M, Knox JE, Cross JB, Bakken V, Adamo C, Jaramillo J, Gomperts R, Stratmann RE, Yazyev O, Austin AJ, Cammi R, Pomelli C, Ochterski JW, Martin RL, Morokuma K, Zakrzewski VG, Voth GA, Salvador P, Dannenberg JJ, Dapprich S, Daniels AD, Farkas O, Foresman JB, Ortiz JV, Cioslowski J, Fox DJ. 2009. Gaussian 09, revision D.01. Gaussian Inc, Wallingford CT.

Hohenstein EG, Chill ST, Sherrill CD. 2008. Assessment of the performance of the M05− 2X and M06−2X exchange-correlation functionals for noncovalent interactions in biomolecules. J Chem Theory Comput. 4(12):1996–2000.

Wang HH, Qiu KM, Cui HE, Yang YS, Luo Y, Xing M, Qiu XY, Bai L.F., Zhu H.L. 2013. Synthesis, molecular docking and evaluation of thiazolyl-pyrazoline derivatives containing benzodioxole as potential anticancer agents. Bioorg Med Chem. 21:448−455.

Kharbanda C, Alam MS, Hamid H, Javed K, Bano S, Dhulap A, Ali Y, Nazreen S., Haider S. 2014. Synthesis and evaluation of pyrazolines bearing benzothiazole as anti-inflammatory agents. Bioorg Med Chem. 22: 5804−5812.

Jorgensen WJ, Duffy EM. 2002. Prediction of drug solubility from structure. Adv Drug Deliv Rev. 54(3):355–366.

Joshi SD, Dixit SR, Kirankumar MN, Aminabhavi TM, Raju KVSN, Narayan R, Lherbet C, Yang KS. 2016. Synthesis, antimycobacterial screening and ligand-based molecular docking studies on novel pyrrole derivatives bearing pyrazoline, isoxazole and phenyl thiourea moieties. Eur J Med Chem. 107:133−152.

Kaplancıklı ZA, Özdemir A, Turan-Zitouni G, Altıntop MD, Can DÖ. 2010. New pyrazoline derivatives and their antidepressant activity. Eur J Med Chem. 45: 4383−4387.

Kim BS, Shin SY, Ahn S, Koh D, Lee YH, Lim Y. 2017. Biological evaluation of 2- pyrazolinyl-1-carbothioamide derivatives against HCT116 human colorectal cancer cell lines and elucidation on QSAR and molecular binding modes. Bioorg Med Chem. 25: 5423−5432.

Kumar S, Bawa S, Drabu S, Kumar R, Gupta H. 2009. Biological activities of pyrazoline derivatives -A recent development. Recent Pat Anti-Infect Drug Discov. 4:154−163.

Lakhrissi Y, Rbaa M, Tuzun B, Hichar A, Ounine K, Almalki F, Hadda TB, Zarrouk A, Lakhrissi B. 2022. Synthesis, structural confirmation, antibacterial properties and bio-informatics computational analyses of new pyrrole based on 8-hydroxyquinoline. J Mol Struct. 1259:132683.

Li HL, Su MM, Xu YJ, Xu C, Yang YS, Zhu HL. 2018. Design and biological evaluation of novel triaryl pyrazoline derivatives with dioxane moiety for selective BRAFV600E inhibition. Eur J Med Chem. 155: 725−735.

Lipinski CA. 2004. Lead-and drug-like compounds: the rule-of-five revolution Drug Discovery Today: Technologies, 1(4): 337–341.

Lipinski CA, Lombardo F, Dominy BW, Feeney PJ. 1997. Experimental and computational approaches to estimate solubility and permeability in drug discovery and development settings. Adv Drug Deliv. Rev. 23:3–25.

Majumdar D, Philip JE, Tüzün B, Frontera A, Gomila RM, Roy S, Bankura K. 2022. Unravelling the Synthetic Mimic, Spectroscopic Insights, and Supramolecular Crystal Engineering of an Innovative Heteronuclear Pb (II)-Salen Cocrystal: An Integrated DFT, QTAIM/NCI Plot, NLO, Molecular Docking/PLIP, and Antibacterial Appraisal. J Inorg Organomet Polym Mater. 1–20.

Majumdar D, Philip JE, Roy S, Tüzün B. 2022. Reinvigorate the synthesis, spectroscopic findings, SEM morphology investigation, and antimicrobial silhouette of contemporary Salen ligands: A comprehensive DFT landscape. Results Chem. 4:100574.

Mathur G, Nain S, Sharma PK. 2015. Cancer: An Overview. Academic Journal of Cancer Research. 8 (1): 01-09.

Marusiak AA, Stephenson NL, Baik H, Trotter EW, Li Y, Blyth K., Mason S, Chapman P, Puto LA, Read JA, Brassington C, Pollard HK, Philips C, Green I, Overman R, Collier M, Testoni E, Miller CJ, Hunter T, Sansom OJ, Brognard J. 2016. Recurrent MLK4 Loss-of-Function Mutations Suppress JNK Signaling to Promote Colon Tumorigenesis. Cancer Res. 76(3):724–735.

Monga V, Goyal K, Steindel M, Rajani DP, Rajani S. 2014. Synthesis, and evaluation of new chalcones, derived pyrazolines and cyclohexenone derivatives as potent antimicrobial, antitubercular and antilieshmanial agents. Med Chem Res. 23: 2019−2032.

Moreno LM, Quiroga J, Abonia R, Ramírez-Prada J, Insuasty B. 2018. Synthesis of new 1,3,5-triazine-based 2-pyrazolines as potential anticancer agents. Molecules. 23:1956.

Nehra B, Rulhania S, Jaswal S, Kumar B, Singh G, Monga V. 2020. Recent advancements in the development of bioactive pyrazoline derivatives. Eur J Med Chem. 205: 112666.

Nepali K, Sharma S, Sharma M, Bedi PMS, Dhar KL. 2014. Rational approaches, design strategies, structure activity relationship and mechanistic insights for anticancer hybrids. Eur J Med Chem. 77:422–487.

Nussbaumer S, Bonnabry P, Veuthey J-L, Fleury-Souverain S. 2011. Analysis of anticancer drugs:A review. Talanta. 85:2265–2289.

Özdemir A, Turan-Zitouni G, Kaplancikli ZA, Revial G, Demirci F, Işcan G. 2010. Preparation of some pyrazoline derivatives and evaluation of their antifungal activities. J Enzym Inhib Med Chem. 25:565−571.

Okamoto K, Ikemori-Kawada M, Jestel A, von König K, Funahashi Y, Matsushima T, Tsuruoka A, Inoue A, Matsui J. 2015. Distinct binding mode of multikinase inhibitor lenvatinib revealed by biochemical characterization. ACS Med Chem Lett. 6(1):89–94.

Rebucci M, Michiels C. 2013. Molecular aspects of cancer cell resistance to chemotherapy. Biochem Pharmacol 85:1219–1226.

Rosenfeld L, Sananes A, Zur Y, Cohen S, Dhara K, Gelkop S, Zeev EB, Shahar A, Lobel L, Akabayov B, Arbely E, Papo N. 2020. Nanobodies targeting prostate-specific membrane antigen for the imaging and therapy of prostate cancer. J Med Chem. 63(14):7601–7615.

Schrödinger Release 2021-3: Maestro, Schrödinger, LLC, New York, NY, 2021.

Schrödinger Release 2019-4: Protein Preparation Wizard; Epik, Schrödinger, LLC, New York, NY, 2016; Impact, Schrödinger, LLC, New York, NY, 2016; Prime, Schrödinger, LLC, New York, NY, 2019.

Schrödinger Release 2021-3: LigPrep, Schrödinger, LLC, New York, NY, 2021.

Schrödinger Release 2021-3: QikProp, Schrödinger, LLC, New York, NY, 2021.

Stefanes NM, Toigo J, Maioral MF, Jacques AV, Chiaradia-Delatorre LD, Perondi DM, Ribeiro AAB, Bigolin A, Pirath IMS, Duarte BF, Nunes RJ, Santos Silva MC. 2019. Synthesis of novel pyrazoline derivatives and the evaluation of death mechanisms involved in their antileukemic activity. Bioorg Med Chem. 27:375−382.

Tas A, Tüzün B, Khalilov AN, Taslim P, Ağbektas T, Cakmak NK. 2022. In Vitro Cytotoxic Effects, In Silico Studies, Some Metabolic Enzymes Inhibition, and Vibrational Spectral Analysis of Novel β-Amino Alcohol Compounds. J Mol Struct. 1273:34282.

Tapera M, Kekeçmuhammed H, Tüzün B, Sarıpınar E, Koçyiğit ÜM, Yıldırım E, Doğan M, Zorlu Y. 2022. Synthesis, carbonic anhydrase inhibitory activity, anticancer activity and molecular docking studies of new imidazolyl hydrazone derivatives. J Mol Struct. 1269 (2022): 133816.

Tüzün B, Sayin K., Ataseven H. 2022. Could Momordica Charantia Be Effective In The Treatment of COVID19? Cumhuriyet Science Journal. 43(2):211–220.

Vautherin D, Brink DM. 1972. Hartree-Fock calculations with Skyrme's interaction. I. Spherical nuclei. Phys Rev C. 5(3):626.

Williams RS, Green R, Glover JN. 2001. Crystal structure of the BRCT repeat region from the breast cancer-associated protein BRCA1. Nat Struct Mol Biol. 8(10):838–842.

Xu W, Pan Y, Wang H, Li H, Peng Q, Wei D, Chen C, Zheng J. 2017. Synthesis and evaluation of new pyrazoline derivatives as potential anticancer agents in HepG-2 cell line. Molecules. 22:467.